PCCP

ARTICLE TYPE

Cite this: DOI: 00.0000/xxxxxxxxxx

Supporting information: Hydrogen Atom Scattering at the $Al_2O_3(0001)$ Surface: A Combined Experimental and Theoretical Study

Martin Liebetrau[1,2], Yvonne Dorenkamp[3], Oliver Bünermann[3,4,5,*] and Jörg Behler[1,2,**]

Received Date
Accepted Date

DOI: 00.0000/xxxxxxxxxx

1 Experiment

1.1 Characterization of the α-$Al_2O_3(0001)$ surface

In the experiments, a $10\times10\times0.5$ mm^3 single crystal purchased from Crystal GmbH was used. Prior to experiment, the surface was investigated by electron energy loss spectroscopy (EELS) and energy dispersive X-ray spectroscopy (EDX) for surface stoichiometry as well as with atomic force microscopy (AFM) for surface roughness, details can be found in Ref. 1. EELS and EDX gave the expected Al:O ratio of 2:3. AFM measurements yielded an average roughness of 0.1 nm, which corresponds to less than a tenth of the height of the unit cell ($c \approx 1.3\,\text{nm}^2$). Over an area of 400×500 nm^2 a maximum height difference of 8.7 nm was determined. Based on the specifications from the manufacturer and the AFM images a number of 2-4 steps per 100 nm has been determined. This corresponds to a step density of 2-4%. The typical step height should be n·c/6 with n=2 according to Ref. 2. Furthermore, due to the crystal structure of α-Al_2O_3 the surface structure is mirrored at every step[3]. It is known that the surface exhibits an ordered arrangement of the steps[2], but the orientation of the steps could not be monitored or controlled in the scattering experiments.

In the ultra high vacuum (UHV) scattering chamber, after bake out, the sample was initially cleaned by annealing at 600 °C in an oxygen atmosphere of 10×10^{-6} mbar for more than 20 h. Before each experiment, the sample was again annealed for 30 min in an oxygen atmosphere. Figure S1 shows the Auger electron spectroscopy (AES) spectrum of the cleaned sample. The peak ratios were used to estimate the stoichiometry, giving a $2:3\pm0.2$ ratio of Al:O. The low energy electron diffraction (LEED) pattern (Figure S2) shows a clear (1×1) structure as expected for a clean surface with a minimum amount of vacancies[4,5]. Based on AES and LEED we conclude that the surface has the (1×1) structure with Al termination and AlO_3Al stacking[6,7]. Figure S2 also shows the $[10\bar{1}0]$ direction which together with the surface normal forms the scattering plane in the presented experiment. In experiment, an angular precision of $\pm2°$ for the azimuthal incidence angle is achieved.

2 Simulations

2.1 Exchange correlation functional

To assess the accuracy of the exchange correlation functional for the generation of the DFT training set for the HDNNP, we calculated the lattice constants and the bulk modulus using the two GGA functionals PBE[8] and RPBE[9] and the hybrid functional PBE0[10] including the Tkatchenko-Scheffler dispersion correction[11] for all tested functionals. The comparison of the obtained values with experimental data is shown in Table S1. PBE0 shows a slightly better description of bulk α-Al_2O_3 with respect to experiment compared to the GGA functionals, but overall the differences are small.

Figure S3 shows two one-dimensional cuts of the potential energy surface for the H-atom on top of the optimized α-Al_2O_3 slab at the sites denoted in the insets of each panel. The insets only show a (1×1) cell, while the calculations were run using (2×2) supercells. For each functional, PBE, RPBE and PBE0, initially the surface structure has been relaxed employing the lattice constants of the respective functional. Then, the surface has been kept frozen for computing the energy curves. While the PBE functional shows better agreement with the hybrid PBE0 functional for the

[1] Lehrstuhl für Theoretische Chemie II, Ruhr-Universität Bochum, D-44780 Bochum, Germany
[2] Research Center Chemical Sciences and Sustainability, Research Alliance Ruhr, D-44780 Bochum, Germany
[3] Georg-August-Universität Göttingen, Institut für Physikalische Chemie, Tammannstraße 6, D-37077 Göttingen, Germany
[4] Department of Dynamics at Surfaces, Max-Planck-Institute for Multidisciplinary Sciences, Am Fassberg 11, D-37007 Göttingen, Germany
[5] International Center of Advanced Studies of Energy Conversion, Georg-August-Universität Göttingen, Tammannstraße 6, D-37077 Göttingen, Germany
* Corresponding Author: oliver.buenermann@chemie.uni-goettingen.de
** Corresponding Author: joerg.behler@rub.de

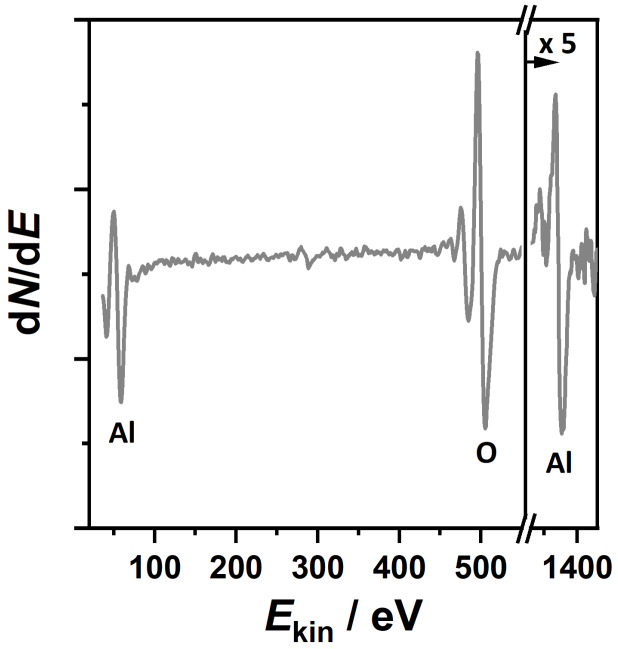

Fig. S1 Auger Electron Spectrum (AES) of the α-Al_2O_3(0001) sample after preparation in the UHV scattering chamber. Peak rations were used to determine the stoichiometry of the surface.

Table S1 The calculated and experimental lattice constants a and c and the bulk modulus B_0 of α-Al_2O_3 [12] for the PBE, RPBE and PBE0 functional in combination with the Tkatchenko-Scheffler dispersion correction [11].

parameter	PBE	RPBE	PBE0	Exp.
a/Å	4.791	4.827	4.738	4.7554 [12]
c/Å	13.072	13.145	12.916	12.991 [12]
B_0/GPa	229	222	258	253 [13]

adsorption well above the oxygen atom in panel b), the RPBE functional provides a better description of the repulsive wall and the adsorption at the Al site in panel a), which is the global minimum for the optimized surface. Since overall the RPBE functional provides a better description of the repulsive walls at much lower costs compared to the PBE0 functional, we have chosen the RPBE functional for constructing the HDNNP in the present work.

2.2 Farthest point sampling

As mentioned in Section 3.3 in the main text, next to active learning also farthest point sampling [14] was used to identify H-atom chemical environments in the trajectories, which are structurally different from the geometries already present in the data set. To identify the structures with the most different chemical environments for the H-atom, the Euclidean distance between the symmetry function vectors of the H-atom in each candidate structure and every symmetry function vector of the H-atoms already included in the data set has been calculated. From this list, the structure with the largest distance was added to the data set, followed by repetitions of the same procedure to determine further geometries. This approach rapidly increased the quality of the

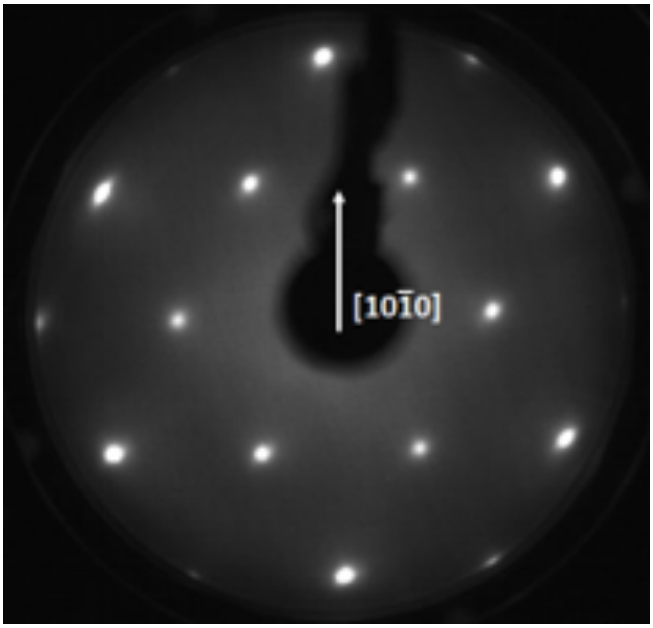

Fig. S2 Low energy electron diffraction (LEED) pattern of the α-Al_2O_3(0001) sample after preparation in the UHV scattering chamber. The scattering plane of the H-atom beam is along the shown $[10\bar{1}0]$ direction.

fit while avoiding the introduction of redundant structures. Typically, structures added this way correspond to hydrogen atom positions close to the surface, as the symmetry function vectors of the H-atom become more similar at large distances from the surface reflecting the decreasing interaction with specific surface sites.

2.3 Hessian analysis of atomic interactions

In the reference data set and in the MD simulations the bottom half of the slab is frozen in the relaxed geometry of the clean slab. For this procedure it has to be ensured that there is no significant interaction between the H-atom and the Al-O_3-Al trilayers in the frozen part of the system. While in the HDNNP this can be achieved by choosing a cutoff radius of the atom-centered symmetry functions, which is smaller than the shortest distance between the frozen atoms and the H-atom in the closest position to the surface, this procedure would only be acceptable if the "true" interactions in DFT are indeed small. This can be tested employing a recently proposed method based on an analysis of the Hessian [15], which corresponds to the derivative of the forces with respect to the atomic positions. Specifically, for a H-atom position very close to the surface, i.e., the case of the largest possible interactions, we computed the Hessian submatrix norm values $||\mathbf{h}_{\mathrm{HX}}||$ between the atoms in the different surface layers and the H-atom. The Hessian submatrix norm is defined as

$$||\mathbf{h}_{\mathrm{HX}}|| = \sqrt{\sum_{\alpha=x,y,z}\sum_{\beta=x,y,z} h^2_{\mathrm{A}_\alpha\mathrm{X}_\beta}}, \quad (1)$$

where A_α are the Cartesian coordinates of the H-atom, X_β are the Cartesian coordinates of the surface atoms and $h_{\mathrm{A}_\alpha\mathrm{X}_\beta}$ describes

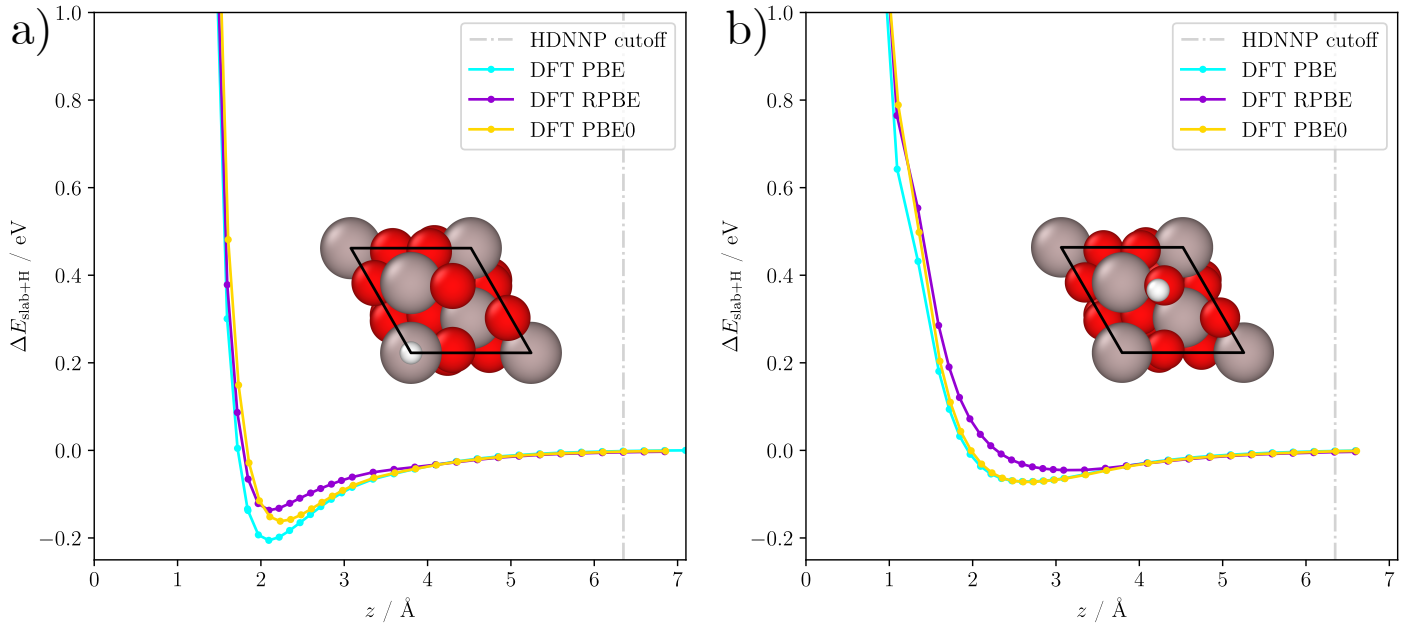

Fig. S3 One-dimensional potential energy curves for a hydrogen atom approaching the frozen relaxed α-Al_2O_3(0001) surface at the sites shown in the insets of a) and b). The energy is shown relative to the energy of the relaxed surface and an infinitely distant hydrogen atom for three different exchange-correlation functionals, PBE[8], RPBE[9] and PBE0[10]. z is the distance of the H atom from the topmost oxygen layer. For comparison, also the typical cutoff radius of 12 Bohr of the atom-centered symmetry functions employed in the HDNNP construction centered at the topmost surface layer is shown.

the interaction between the H-atom and a surface atom X in form of a 3×3 submatrix of the Hessian matrix. The results are shown in Fig. S4, and beyond a distance of about 8 Å, i.e., in the deep frozen layers, the remaining interactions are very small as indicated by a submatrix norm below $0.2\,\mathrm{eV\,Å^{-2}}$.

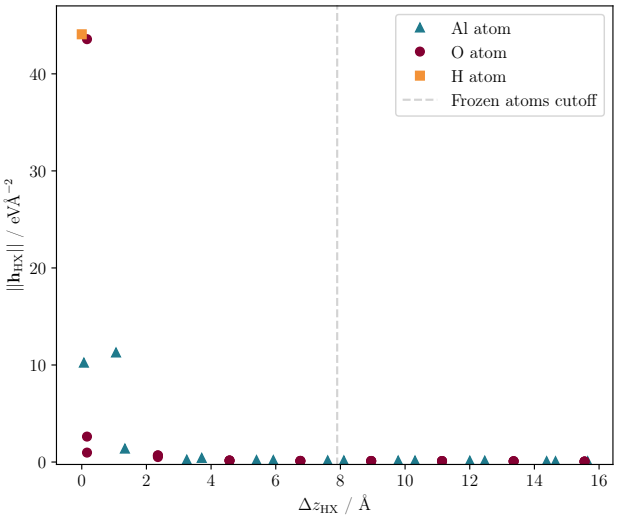

Fig. S4 Hessian analysis of the influence of atoms in the slab on the H-atom, which is in close proximity to the surface. The atomic Hessian submatrix norm value $||\mathbf{h}_{\mathrm{HX}}||$ for each atom is plotted vs. Δz, the distances in z direction from the H-atom, which is located at $z = 0$. The frozen layers start at a distance of 7.9 Å, which is shown by the dashed grey line.

2.4 HDNNP parameters

The parameters of the atom-centered symmetry functions for the description of the atomic environments are given in Table S2 for the radial functions and in Table S3 for the angular functions. For simplicity Table S3 shows only those angular functions, which have NOT been used from a pool including all permutations of the parameters $\lambda = \{-1, 1\}$, $\zeta = \{1, 2, 4, 16\}$, and $\eta = \{0, 0.05\}$ a_0^{-2} (for a discussion of these parameters see Ref. 16). Moreover, ACSFs refering to interactions between hydrogen atoms have been omitted, since these interactions are not present here. The general input settings for the RuNNer code are given in Table S4.

Table S2 Parameters η of the employed radial atom-centered symmetry functions.

Element pair	$\eta\,/\,a_0^{-2}$
H-O	0, 0.005, 0.013, 0.029, 0.067, 0.187
O-H	0, 0.005, 0.013, 0.029, 0.067, 0.187
H-Al	0, 0.005, 0.012, 0.027, 0.058, 0.145
Al-H	0, 0.005, 0.012, 0.027, 0.058, 0.145
O-O	0, 0.005, 0.011, 0.023, 0.048, 0.109
O-Al	0, 0.004, 0.010, 0.019, 0.036, 0.070
Al-O	0, 0.004, 0.010, 0.019, 0.036, 0.070
Al-Al	0, 0.003, 0.008, 0.014, 0.024, 0.041

Table S3 List of angular ACSFs, which have not been used in the training process starting from a pool of all combinations of the parameters $\lambda = \{-1,1\}$, $\zeta = \{1,2,4,16\}$, and $\eta = \{0,0.05\}$ a_0^{-2}.

Element triple	$\eta\,/\,a_0^{-2}$	λ	ζ
H-Al-Al	0.05	1	16
H-Al-Al	0.05	-1	16
Al-Al-Al	0.05	1	16
Al-Al-H	0.05	1	16
Al-Al-Al	0.05	-1	16
Al-Al-H	0.05	-1	16

Table S4 Settings in the RuNNer input file for constructing the HDNNP (specification of the ACSFs have been left out).

	Value
nn_type_short	1
random_number_type	5
random_seed mode 1	13242
random_seed mode 2	37198
number_of_elements	3
elements	H O Al
remove_atom_energies atom_energy H / E_h	-0.50498442
atom_energy O / E_h	-75.16628513
atom_energy Al / E_h	-243.03908176
energy_threshold	-0.215
bond_threshold	0.5
cutoff_type	1
use_short_nn	
global_hidden_layers_short	2
global_nodes_short	15 15
global_activation_short	t t l
test_fraction	0.1
epochs	20
points_in_memory	20000
mix_all_points	
scale_symmetry_functions	
center_symmetry_functions	
fitting_unit	eV
precondition_weights	
use_short_forces	
optmode_short_energy	1
optmode_short_force	1
kalman_lambda_short	0.98
kalman_nue_short	0.9987
element_decoupled_kalman	
short_energy_fraction	1.0
short_force_fraction	0.025
weights_min	-0.5
weights_max	0.5
nguyen_widrow_weights_short	
short_energy_error_threshold	0.0
short_force_error_threshold	0.2
force_update_scaling	1.5
max_force	0.11

2.5 HDNNP accuracy

The reference data set consists of 15,812 structures, which include 808 bulk structures and 15,004 slab structures, of which 2,300 do not contain a H-atom. The HDNNP has a RMSE for the testing data set of $0.746\,\mathrm{meV\,atom^{-1}}$ for the energy and $0.103\,\mathrm{eV\AA^{-1}}$ for the atomic force components. For the training set the RMSE values are $0.257\,\mathrm{meV\,atom^{-1}}$ for the energy and $0.111\,\mathrm{eV\AA^{-1}}$ for the force components. The largest energy error is $5.47\,\mathrm{meV\,atom^{-1}}$. The energy RMSE is well below the typical target error for machine learning potentials of about $1\,\mathrm{meV\,atom^{-1}}$. Figures S5 and S6 show the absolute prediction error for the training and testing set, respectively. The error is plotted against the DFT binding energy. Figures S7 and S8 show the prediction error for the force components.

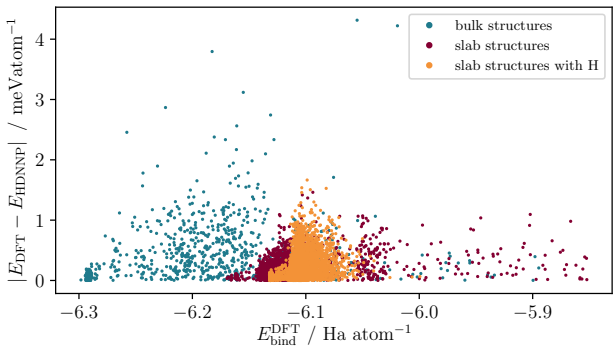

Fig. S5 Absolute HDNNP prediction error $\Delta E = |E_{DFT} - E_{HDNNP}|$ of the training set plotted vs. the DFT binding energy of the structure. The points are colored by type of structure, bulk, clean slab and slab with H-atom.

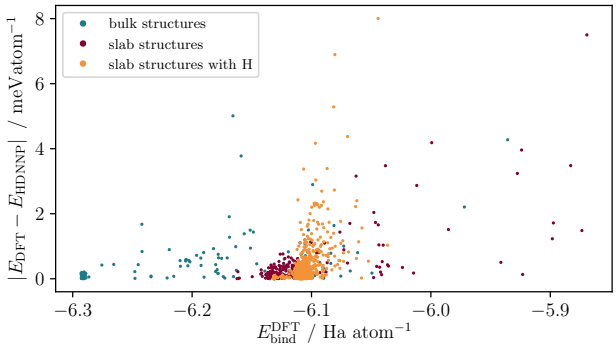

Fig. S6 Absolute HDNNP prediction error $\Delta E = |E_{DFT} - E_{HDNNP}|$ of the testing set plotted vs. the DFT binding energy of the structure. The points are colored by type of structure, bulk, clean slab and slab with H-atom. The maximum prediction error is roughly twice as large as the maximum error of the training set (Figure S5), but most of the structures are described with an accuracy comparable to the training set.

2.6 Azimuthal incident angle

The α-$Al_2O_3(0001)$ surface has two energetically equivalent surface terminations, which are related by a mirror operation. They correspond to different layers of the material, as shown in the side and top views in Figure S9. The lighter colored side on

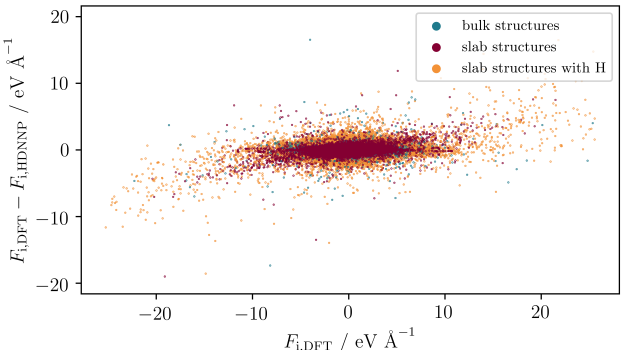

Fig. S7 HDNNP prediction error $\Delta F_i = F_{i,\mathrm{DFT}} - E_{i,\mathrm{HDNNP}}$ of the training set for each Cartesian force component i plotted vs. the DFT force component. The points are colored by type of structure, bulk, clean slab and slab with H-atom.

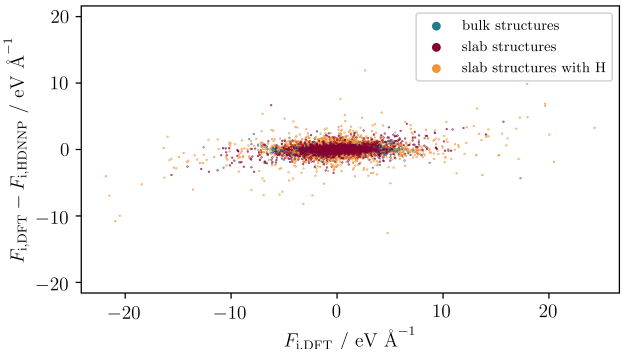

Fig. S8 HDNNP prediction error $\Delta F_i = F_{i,\mathrm{DFT}} - E_{i,\mathrm{HDNNP}}$ of the testing set for each Cartesian force component i plotted vs. the DFT force component. Force error distributions are very similar to the training set (s. Fig. S7) indicating good transferability.

the left shows the top trilayer, which is removed for the lower darker colored side on the right. In the top view of panel (b) the different orientation of the AlO_3 units can be clearly seen. Since in experiment the existence of steps is unavoidable, scattering can be assumed to occur on both surfaces, which has to be taken into account in the simulations by combining scattering from both surfaces. This is done by averaging for scattering H-atom with azimuthal angles of ϕ_i=0° and ϕ_i=180°. Figures S10 to S13 show the scattering for ϕ_i=0° and ϕ_i=180° separately for all experimental incident conditions, starting with $E_{\mathrm{kin,i}} = 0.99\,\mathrm{eV}$ and $\theta_\mathrm{i} = 40°$ in figure S10, $E_{\mathrm{kin,i}} = 1.92\,\mathrm{eV}$ and $\theta_\mathrm{i} = 40°$ in figure S11, $E_{\mathrm{kin,i}} = 0.99\,\mathrm{eV}$ and $\theta_\mathrm{i} = 55°$ in figure S12 and $E_{\mathrm{kin,i}} = 1.92\,\mathrm{eV}$ and $\theta_\mathrm{i} = 55°$ in figure S13. While there is nearly no difference for scattering with an initial kinetic energy $E_{\mathrm{kin,i}} = 0.99\,\mathrm{eV}$, for the scattering at $E_{\mathrm{kin,i}} = 1.92\,\mathrm{eV}$ the surface termination has a significant influence on the shape of the distribution.

2.7 Detector angle in the simulations

For the determination of the kinetic energy and angular distributions, the incident conditions of the H-atom and the position and velocity at the end of the trajectory are used to decide if the trajectory is to be considered in the respective distributions. If at the end of the trajectory the H-atom has a momentum away from the surface at a distance of at least 7.8 Å it is considered as a scattered atom. For hitting the detector, the velocity vector $\vec{v}_{\mathrm{H,s}}$ has to point towards the same direction as the detector, which is represented by a unit vector $\hat{d}_{\mathrm{detector}}$. The relation between the x and y components of the $\hat{d}_{\mathrm{detector}}$ and the z component of the H-atom velocity vector can be determined from the experimental detector polar angle Θ_{det} as

$$z = \cos\Theta_{\mathrm{det}}\ , \tag{2}$$

$$\sqrt{x^2+y^2} = \sin\Theta_{\mathrm{det}}\ , \tag{3}$$

and the relation between the x and y component can be determined by the experimental detector azimuth angle ϕ_{det} as

$$x = \sin\Theta_{\mathrm{det}} \cdot \cos\phi_{\mathrm{det}}\ , \tag{4}$$

$$y = \sin\Theta_{\mathrm{det}} \cdot \sin\phi_{\mathrm{det}}\ . \tag{5}$$

Combining equations 3.6 -3.9, $\hat{d}_{\mathrm{detector}}$ is given by

$$\hat{d}_{\mathrm{detector}} = \begin{pmatrix} \sin\Theta_{\mathrm{det}} \cdot \cos\phi_{\mathrm{det}} \\ \sin\Theta_{\mathrm{det}} \cdot \sin\phi_{\mathrm{det}} \\ \cos\Theta_{\mathrm{det}} \end{pmatrix}$$

The H-atom velocity vector at the end of the trajectory $\vec{v}_{\mathrm{H,s}}$, and its unit vector $\hat{v}_{\mathrm{H,s}}$, can be used to calculate the difference

$$\gamma = \cos^{-1}\left(\hat{v}_{\mathrm{H,s}} \cdot \hat{d}_{\mathrm{detector}}\right) \tag{6}$$

between the H-atom velocity vector $\hat{v}_{\mathrm{H,s}}$ and the detector position unit vector $\hat{d}_{\mathrm{detector}}$.

In experiment the maximum deviation γ between both vectors is determined by the size of the detector and its distance from the surface, resulting in an angular resolution of 3° yielding $\gamma = 1.5°$. For the theoretical kinetic energy distributions, the threshold for γ can be adjusted to increase or decrease the amount of trajectories needed to obtain statistically meaningful spectra due to the limited number of trajectories hitting the detector. Setting $\gamma = 5°$ increases the amount of counted trajectories by a factor of 10, while not changing the distribution, as shown in Figure S14. As there are less trajectories contributing to the distribution using a value of $\gamma = 1.5°$ resulting in a higher degree of statistical noise in the distribution, the overall shape is the same for the distribution obtained using $\gamma = 5°$.

2.8 Efficient energy transfer trajectory

Figure S15 shows an example trajectory for the case of a very efficient energy transfer to the surface. The trajectory shown corresponds to the incident conditions, slab positions and velocities of the MD1 trajectory listed in the main paper table 2. The trajectory shown has been calculated using the HDNNP. In panel b) the absolute kinetic energy of the H-atom (in black) and the differences in kinetic energies for selected atoms between a trajectory with the scattering H-atom and an unperturbed reference trajectory without the H-atom are shown. The kinetic energy of the

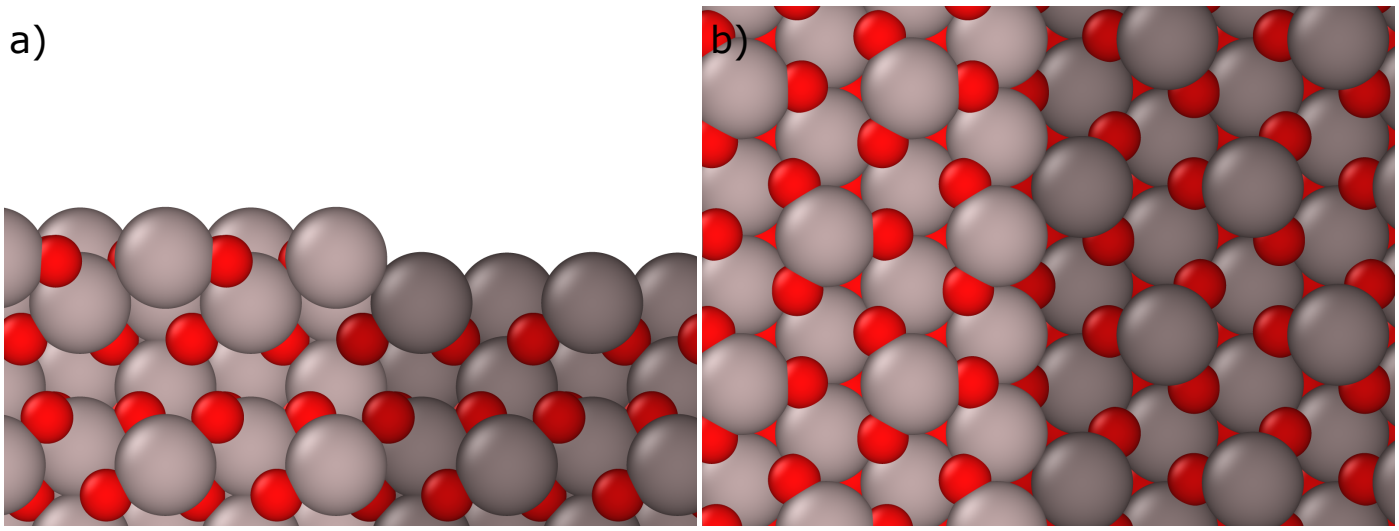

Fig. S9 Side (a) and top (b) view of the two possible surface terminations of the α-Al_2O_3(0001) surface, which are related by a mirror symmetry operation. For the darker atoms on the right of both panels the top trilayer has been removed (without relaxing the surface here for illustration purposes). Al atoms are grey and O atoms are red. Figures created using ovito version 3.8.4 [17].

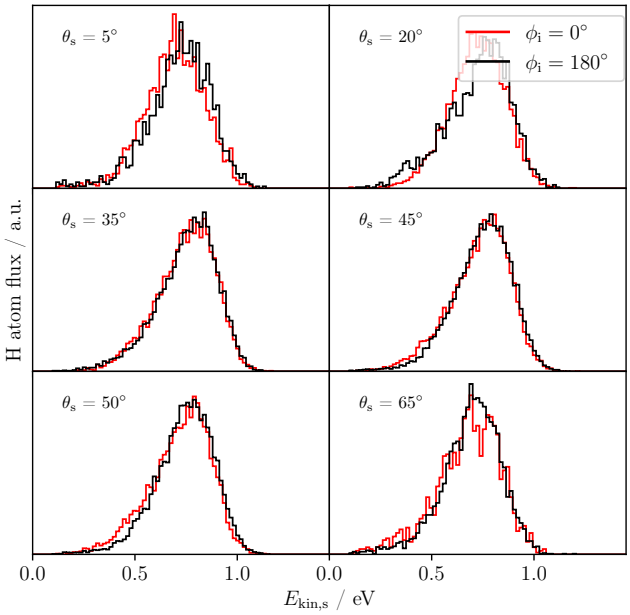

Fig. S10 Kinetic energy distribution plots for $E_{kin,i} = 0.99\,eV$ and $\theta_i = 40°$. The red line shows the scattering with a incident azimuthal angle of $\phi_i = 0°$, while the black line shows the scattering at $\phi_i = 180°$. θ_s is the scattering angle.

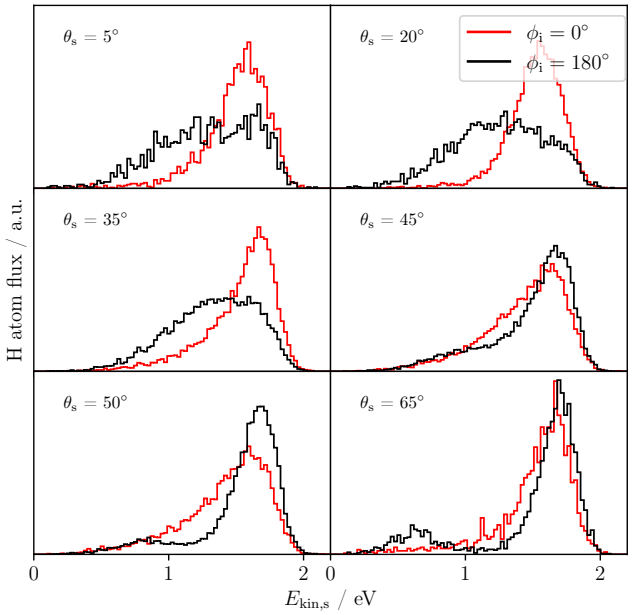

Fig. S11 Kinetic energy distribution plots for $E_{kin,i} = 1.92\,eV$ and $\theta_i = 40°$. The red line shows the scattering with a incident azimuthal angle of $\phi_i = 0°$, while the black line shows the scattering at $\phi_i = 180°$. θ_s is the scattering angle.

H-atom is transferred in a complex mechanism to multiple surface atoms. The impact site is located between Al^1 and O^3, which is why initially a lot of kinetic energy is transferred to O^3 along the impact vector. Moreover, the kinetic energy of O^2, and to a lesser extent of the more distant O^1, increases, which is transmitted via Al^1 such that in total a substantial part of the H-atom kinetic energy is transferred to a AlO_3 unit at the surface. This phenomenon hinders the transfer of kinetic energy back towards the H-atom, once it leaves the surface and increases the kinetic energy loss of the-H atom.

3 Kinetic energy distributions for $\theta_i = 55°$

Figure S16 shows the kinetic energy distribution of the scattered H-atoms scattered at $E_{kin,i}$ =0.99 eV and $\theta_i = 55°$ in panel a) and $E_{kin,i}$ =1.92 eV and $\theta_i = 55°$ in panel b). The theoretical distributions are averaged for the scattering at ϕ_i=0° and ϕ_i=180°.

Notes and references

1 Y. Dorenkamp, C. Volkmann, V. Roddatis, S. Schneider, A. M. Wodtke and O. Bünermann, *J. Phys. Chem. C*, 2018, **122**, 10096.

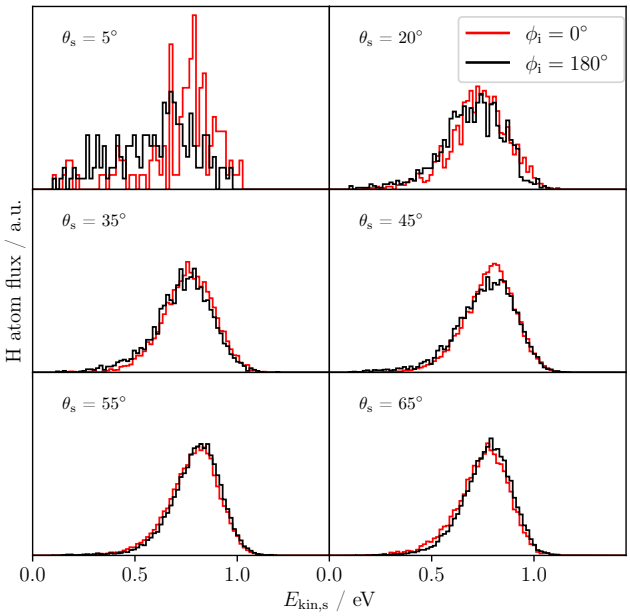

Fig. S12 Kinetic energy distribution plots for $E_{kin,i} = 0.99\,eV$ and $\theta_i = 55°$. The red line shows the scattering with a incident azimuthal angle of $\phi_i = 0°$, while the black line shows the scattering at $\phi_i = 180°$. θ_s is the scattering angle.

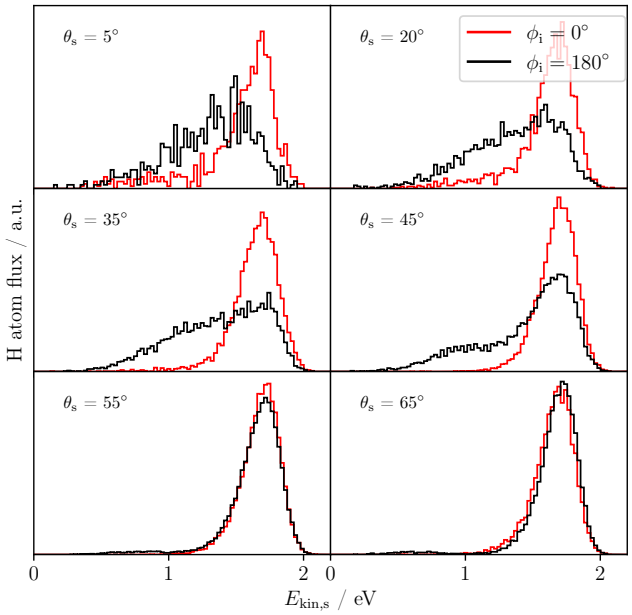

Fig. S13 Kinetic energy distribution plots for $E_{kin,i} = 1.92\,eV$ and $\theta_i = 55°$. The red line shows the scattering with a incident azimuthal angle of $\phi_i = 0°$, while the black line shows the scattering at $\phi_i = 180°$. θ_s is the scattering angle.

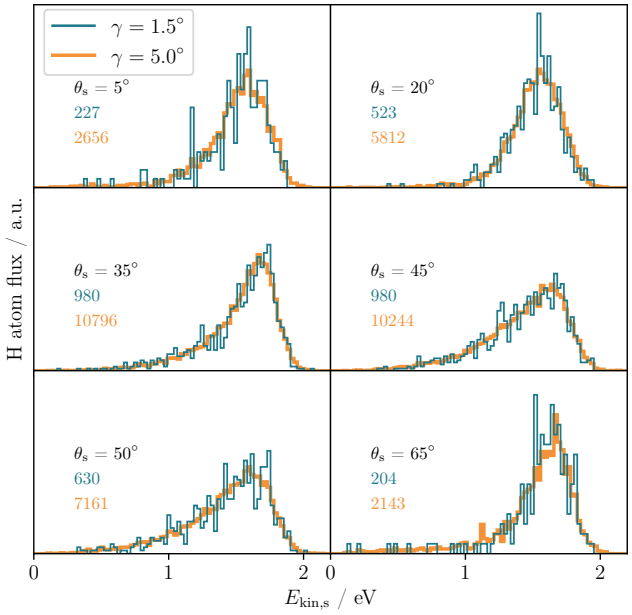

Fig. S14 Kinetic energy distribution plots for $E_{kin,i} = 1.92\,eV$, $\theta_i = 40°$ and $\phi_i = 0°$. The orange line shows the distribution for $\gamma = 5°$ and the blue line for $\gamma = 1.5°$. The number of trajectories hitting the detector at the corresponding θ_s is given in the plot, color coded for the respective γ.

2 L. Van, O. Kurnosikov and J. Cousty, *Surf. Sci.*, 1998, **411**, 263.
3 M. Yoshimoto, T. Maeda, T. Ohnishi, H. Koinuma, O. Ishiyama, M. Shinohara, M. Kubo, R. Miura and A. Miyamoto, *Appl. Phys. Lett.*, 1995, **67**, 2615.
4 C. C. Chang, *J. Appl. Phys.*, 1968, **39**, 5570.
5 D. P. Woodruff, *Chem. Rev.*, 2013, **113**, 3863.
6 J. Ahn and J. Rabalais, *Surf. Sci.*, 1997, **388**, 121.
7 G. Renaud, *Surf. Sci. Rep.*, 1998, **32**, 1.
8 J. P. Perdew, K. Burke and M. Ernzerhof, *Phys. Rev. Lett.*, 1996, **77**, 3865.
9 B. Hammer, L. B. Hansen and J. K. Nørskov, *Phys. Rev. B*, 1999, **59**, 7413.
10 C. Adamo and V. Barone, *J. Chem. Phys.*, 1999, **110**, 6158.
11 A. Tkatchenko and M. Scheffler, *Phys. Rev. Lett.*, 2009, **102**, 073005.
12 X.-L. Wang, C. R. Hubbard, K. B. Alexander, P. F. Becher, J. A. Fernandez-Baca and S. Spooner, *J. Am. Ceram. Soc.*, 1994, **77**, 1569.
13 D. L. Anderson and O. L. Anderson, *J. Geophys. Res.*, 1970, **75**, 3494.
14 Y. Eldar, M. Lindenbaum, M. Porat and Y. Zeevi, *IEEE Trans. Image Process.*, 1997, **6**, 1305.
15 M. Herbold and J. Behler, *J. Chem. Phys.*, 2022, **156**, 114106.
16 J. Behler, *J. Chem. Phys.*, 2011, **134**, 074106.
17 A. Stukowski, *Model. Simul. Mater. Sci. Eng.*, 2010, **18**, 015012.

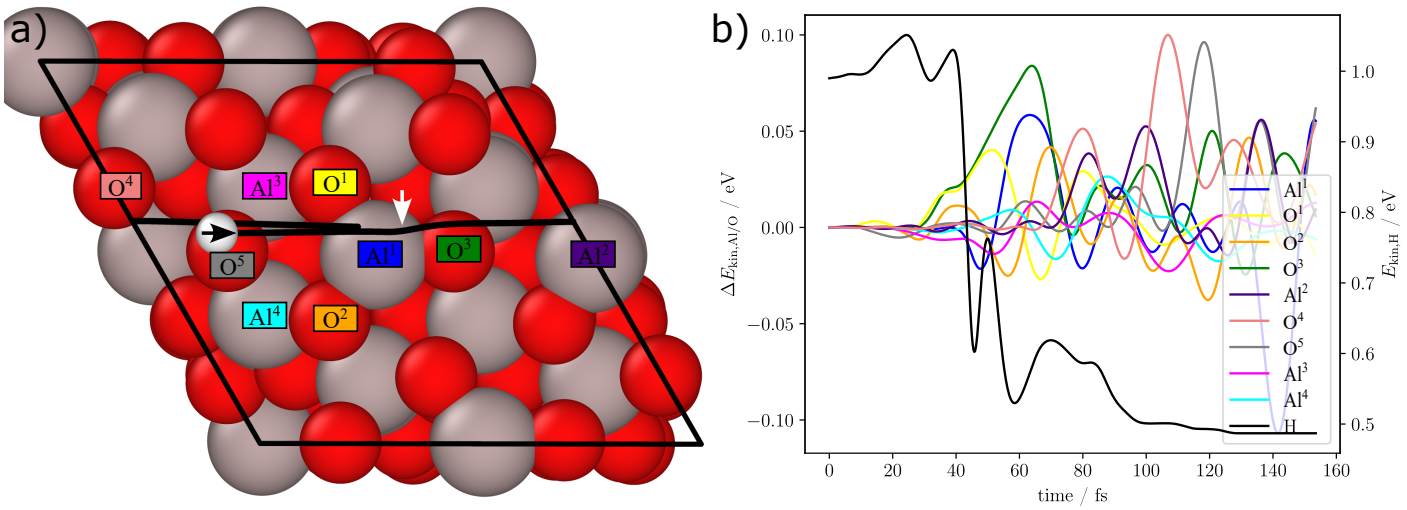

Fig. S15 Example trajectory for the case of an efficient kinetic energy transfer from the H-atom to the surface, corresponding to the incident conditions, slab positions and velocities of the MD1 trajectory listed in the main paper table 2. Panel a) shows the trajectory of the H-atom in black on top of the surface, for which the initial atomic positions at the beginning of the trajectory are shown. The surface atoms are mobile and are equilibrated at 300 K. The white arrow denotes the closest position of the H-atom to the surface and the black arrow shows the direction of the H atom. Panel b) shows the difference between the kinetic energy of the surface atoms from trajectories calculated with the scattering H-atom and an unperturbed reference trajectory without the H-atom to highlight the changes in the surface motions induced by the atomic impact. The black line shows the absolute kinetic energy of H-atom.

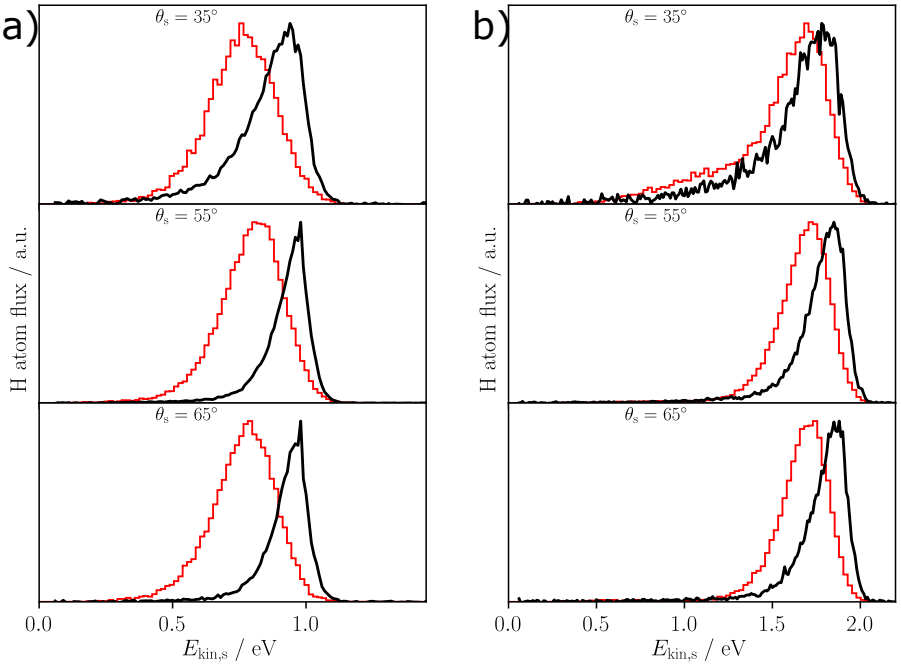

Fig. S16 Kinetic energy loss distributions for H-atom scattering at a) $E_{\mathrm{kin,i}}$ =0.99 eV and $\theta_{\mathrm{i}} = 55°$, b) $E_{\mathrm{kin,i}}$ =1.92 eV and $\theta_{\mathrm{i}} = 55°$. The black line shows the experimentally measured distributions, while the red line shows the theoretical distributions. The detected scattering polar angle θ_{s} is given in each panel. All distributions have been normalized to a maximum of one.